Kinetic Mechanism of *Tritrichomonas foetus* Inosine 5′-Monophosphate Dehydrogenase†

Jennifer A. Digits and Lizbeth Hedstrom*

Department of Biochemistry, Brandeis University, Waltham, Massachusetts 02454

Received September 24, 1998; Revised Manuscript Received December 9, 1998

ABSTRACT: IMP dehydrogenase (IMPDH) catalyzes the oxidation of IMP to XMP with conversion of NAD^+ to NADH. This reaction is the rate-limiting step in de novo guanine nucleotide biosynthesis. IMPDH is a target for antitumor, antiviral, and immunosuppressive chemotherapy. We have determined the complete kinetic mechanism for IMPDH from *Tritrichomonas foetus* using ligand binding, isotope effect, pre-steady-state kinetic, and rapid quench kinetic experiments. Both substrates bind to the free enzyme, which suggests a random mechanism. IMP binds to the enzyme in two steps. Two steps are also involved when IMP binds to a mutant IMPDH in which the active site Cys is substituted with a Ser. This observation suggests that this second step may be a conformational change of the enzyme. No V_m isotope effect is observed when [2-^{2}H]IMP is the substrate which indicates that hydride transfer is not rate-limiting. This result is confirmed by the observation of a pre-steady-state burst of NADH production when monitored by absorbance. However, when NADH production was monitored by fluorescence, the rate constant for the exponential phase is 5−10-fold lower than when measured by absorbance. This observation suggests that the fluorescence of enzyme-bound NADH is quenched and that this transient represents NADH release from the enzyme. The time-dependent formation and decay of [^{14}C]E−XMP* intermediates was monitored using rapid quench kinetics. These experiments indicate that both NADH release and E−XMP* hydrolysis are rate-limiting and suggest that NADH release precedes hydrolysis of E−XMP*.

IMP dehydrogenase (IMPDH)[1] catalyzes the oxidation of IMP to XMP with the conversion of NAD^+ to NADH. This reaction is the rate-limiting step in de novo guanine nucleotide biosynthesis. IMPDH inhibitors have antiproliferative activity. Thus, IMPDH is a target for antitumor, antiviral, and immunosuppressive chemotherapy (*1*−*4*). The activities of the antitumor drug tiazofurin, the antiviral drug ribavirin, and the immunosuppressive drug mycophenolic acid (MPA) are due to the inhibition of IMPDH (*5*−*7*). Furthermore, differences between mammalian and microbial IMPDHs suggest that species-specific inhibitors could be useful for anti-infective chemotherapy (*8*, *9*).

The IMPDH reaction proceeds via attack of Cys319 (*Tritrichomonas foetus* numbering) on the 2-position of IMP (Figure 1). Hydride transfer from the E−IMP intermediate to NAD^+ follows, forming an E−XMP* intermediate. This covalent intermediate is hydrolyzed to XMP, regenerating the free enzyme (*10*, *11*). The reaction is irreversible. Early studies suggested that IMPDH follows an ordered bi-bi kinetic mechanism in which IMP is the first substrate bound and XMP is the last product released. These conclusions were based on product inhibition patterns from various enzyme sources (*9*, *12*−*15*), as well as ligand binding studies (*16*). More recent studies with the human type II IMPDH suggest that the kinetic mechanism proceeds via a random addition of substrates and ordered release of products, with NADH release preceding hydrolysis of E−XMP* (*17*, *18*). In addition, for human IMPDH, hydride transfer and NADH release are fast and hydrolysis of E−XMP* is rate-limiting (*17*).

IMPDH has been isolated from many sources. All are homotetramers with subunit molecular masses of 43−58 kDa. The monomer has an α/β barrel structure (*19*, *20*). Each monomer contains one active site, and each active site binds IMP and NAD^+ (*15*, *21*). IMPDH also contains a loop after β-8, which forms a flap. This flap region is disordered in all crystal structures of IMPDH (*19*, *20*).

T. foetus is an anaerobic protozoan parasite that infects the urogenital tract of cows. The gene for *T. foetus* IMPDH encodes a protein of 503 amino acids whose sequence is 30−35% identical with those of other IMPDHs (*22*). This IMPDH has unique intrinsic protein fluorescence and convenient kinetic properties (low K_m values for both substrates). Like other microbial IMPDHs, the *T. foetus* enzyme differs from mammalian IMPDHs in its resistance to the inhibitor mycophenolic acid (K_{ii} = 9 μM vs K_{ii} = 0.02 μM for human IMPDH) (*23*). Such species selectivity is important in the development of antimicrobial agents. MPA

† Supported by NIH Molecular Structure and Function Training Grant GM07956 (J.A.D.), NIH Grant GM54403 (L.H.), and a grant from the Markey Charitable Trust to Brandeis University.

* To whom correspondence should be addressed. E-mail: hedstrom@brandeis.edu.

[1] Abbreviations: IMPDH, inosine 5′-monophosphate dehydrogenase; IMP, inosine 5′-monophosphate; NAD^+, nicotinamide adenine dinucleotide; NADH, reduced nicotinamide adenine dinucleotide; XMP, xanthosine 5′-monophosphate; APAD, 3-acetylpyridine adenine dinucleotide; APADH, reduced 3-acetylpyridine adenine dinucleotide; GMP, guanosine 5′-monophosphate; MPA, mycophenolic acid; EICARMP, 5-ethynyl-1-β-D-ribofuranosylimidazole-4-carboxamide 5′-monophosphate; DTT, dithiothreitol.

10.1021/bi982305k CCC: $18.00
Published on Web 02/05/1999

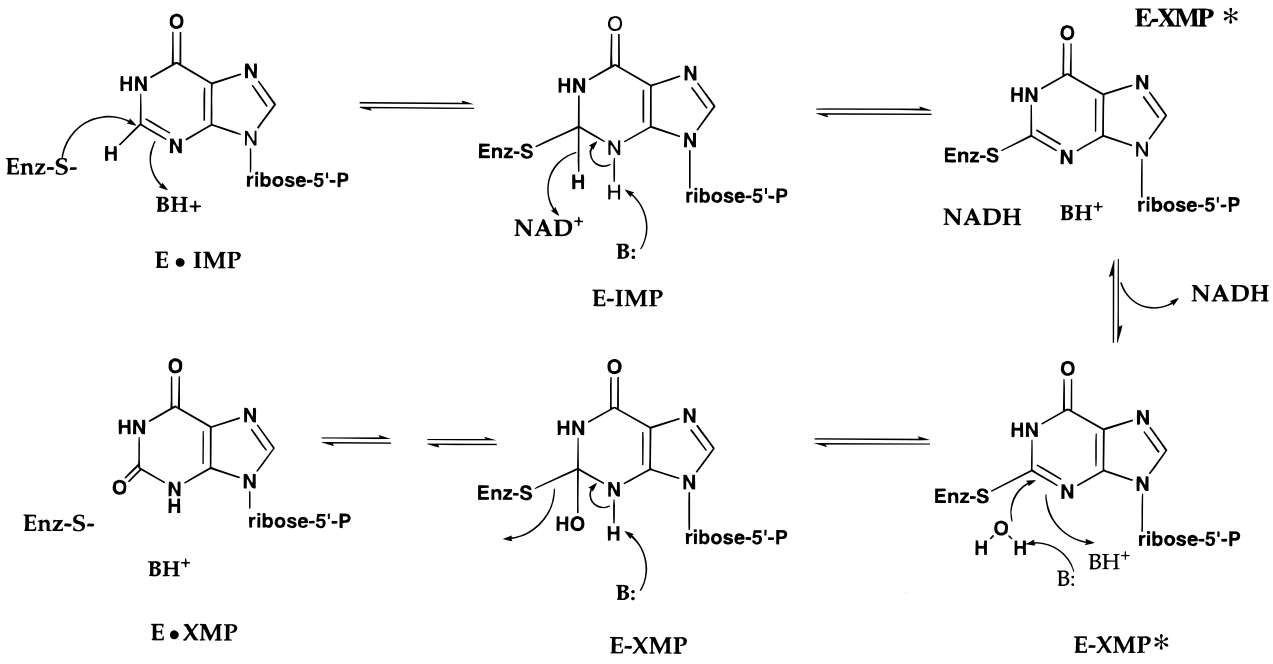

FIGURE 1: Mechanism of the IMPDH reaction.

binds to E−XMP* (*11*, *19*, *24*−*26*). Therefore, both the affinity of E−XMP* for MPA and the accumulation of E−XMP* will determine the MPA sensitivity. Since the hydrolysis of E−XMP* is rate-limiting for human IMPDH, E−XMP* will be the predominant enzyme complex during steady state. Therefore, human IMPDH is primarily in the MPA sensitive form. The values of k_{cat} for microbial IMPDHs are 3−30-fold higher than that of human IMPDH. This observation indicates that the rate of hydrolysis of E−XMP* must also be at least 3−30 times greater in microbial IMPDHs. Therefore, E−XMP* hydrolysis may no longer be rate-limiting in the reaction of microbial IMPDHs, and E−XMP* may no longer be the predominant enzyme form. In this case, MPA resistance could result from the failure to accumulate E−XMP*. Thus, a complete understanding of the kinetic mechanisms of IMPDHs from both microbial and mammalian sources is important for specific inhibitor design.

Here we report a kinetic mechanism for *T. foetus* IMPDH. These studies indicate that, as in the case for human type II IMPDH, substrates associate randomly and product release is ordered, with NADH release preceding E−XMP* hydrolysis. However, unlike the mechanism for human IMPDH, NADH release is partially rate-limiting.

MATERIALS AND METHODS

Materials. IMP, XMP, NADH, GMP, APAD, and Tris were purchased from Sigma. NAD^+ was purchased from Boehringer Mannheim. DTT was purchased from Research Organics, Inc. Glycerin, EDTA, and KCl were purchased from Fisher. [8-^{14}C]IMP was obtained from Moravek Biochemicals, Inc. The plasmid pBimpdh containing the *T. foetus* gene was a gift from C. C. Wang (University of California, San Francisco). The plasmid pKK223-3 was purchased from Pharmacia. EICARMP was a gift from A. Matsuda (Hokkaido Univ., Japan). Oligonucleotides were obtained from the Brandeis Oligonucleotide Facility.

Synthesis of [2-^{2}H]IMP. [2-^{2}H]IMP was synthesized and purified as previously described (*17*).

Construction of an Expression System for T. foetus IMPDH. The *Hin*dIII restriction site was removed by inserting a silent mutation in the *T. foetus* gene using the Quikchange kit (Stratagene, La Jolla, CA) with pBimpdh as a template. The resulting DNA was amplified by PCR to insert convenient restriction sites at the beginning and end of the *T. foetus* gene. The following oligonucleotides were used (restriction sites are bold). ACC-AGC-CAA-**GAA-TTC**-ATG-GCA-AAA-TAC-TAC-AAC-GAA-CCA-TGC-CAC inserts an *Eco*RI site at the 5′ end, and ACC-AGC-CAA-**AAG-CTT**-TTA-TTT-TGG-GTG-ATA-GTC-GTT-AAT-CCT-GTC inserts a *Hin*dIII site in the 3′ noncoding region. The *T. foetus* IMPDH coding sequence was amplified with Vent DNA polymerase (New England Biolabs). The amplified DNA fragment was digested with *Eco*RI and *Hin*dIII, purified via agarose gel electrophoresis followed by GeneClean (BIO 101, Inc.), and ligated to the *Eco*RI/*Hin*dIII-digested pKK223-3. The resulting construct is designated pTf1. The *T. foetus* IMPDH coding sequence of pTf1 was completely sequenced using a PRISM Dyedeoxy Terminator Cycle Sequencing kit (Applied Biosystems, Inc.) and an Applied Biosystems 373A DNA sequencer at the Brandeis Sequencing Facility. One undesired silent mutation was created; G was mutated to C at position 867, which still encodes for an Ala at residue 289.

Expression and Purification of T. foetus IMPDH. pTf1 was transformed into H712 cells, which lack *Escherichia coli* IMPDH (*27*). Cells were grown overnight (16−18 h) in 2 L of LB broth with 100 μg/mL ampicillin and 1 mM IPTG at 37 °C while the mixture was shaken constantly. The cells were harvested by centrifugation and washed three times in 50 mM Tris (pH 7.5), 1 mM DTT, and 10% glycerol (buffer A), resuspended in 40 mL of buffer A, and frozen at −80 °C. Cells were lysed by sonication, and cell debris was removed by centrifugation at 10 000 rpm for 30 min. The supernatant was applied to a Cibacron Blue Sepharose column (Sigma) previously equilibriated in buffer A at 4 °C. IMPDH was eluted in a linear gradient of 0 to 2 M KCl in buffer A. Fractions containing IMPDH activity were pooled

and dialyzed against buffer A and 500 μM IMP overnight at 4 °C. IMPDH was further purified on a POROS CM weak cation exchange column using a BioCAD SPRINT perfusion chromatography system (PerSeptive Biosystems, Framingham, MA). Enzyme was eluted in a linear gradient of 0 to 1 M NaCl in 7 mM HEPES, 7 mM MES, and 7 mM sodium acetate buffer containing 1 mM DTT (pH 6.0). Fractions containing IMPDH were pooled, dialyzed against buffer A overnight at 4 °C, and stored at −80 °C. The enzyme preparations were >95% pure as judged by SDS−PAGE. The protein concentration was measured using the Bio-Rad assay with IgG as a standard. Active sites were titrated with EICARMP (*21*).

Mutagenesis. Cys319Ser was constructed from pTf1 using the Quikchange kit. The following oligonucleotides were used (point mutations are bold). GGT-GGA-TCA-ATT-**AGC**-ATC-ACA-CGC is complementary to the noncoding strand of the vector, and GCG-TGT-GAT-**GCT**-AAT-TGA-TCC-ACC is complementary to the coding strand of the vector. The coding sequence of the IMPDH gene was sequenced to ensure no undesired mutations had been introduced.

Enzyme Kinetics. Standard IMPDH assays contained 100 mM KCl, 3 mM EDTA, 1 mM DTT, and 50 mM Tris (pH 8.0) (assay buffer). Activity was assayed in the presence of 100 μM IMP and 1 mM NAD^+ at 25 °C. The production of NADH was monitored spectrophotometrically at 340 nm (ϵ = 6.22 mM^{-1} cm^{-1}) using a Hitachi U-2000 spectrophotometer or a Hewlett-Packard 8453 diode array spectrophotometer. The production of APADH was monitored at 363 nm (ϵ = 9.1 mM^{-1} cm^{-1}). The concentrations of IMP and NAD^+ or its analog were varied for K_m determinations. Initial velocity data were fit to the Michaelis−Menten equation (eq 1) and an uncompetitive substrate inhibition equation (eq 2) using Kaleidagraph software (Abelbeck Software):

$$v = V_m[IMP]/(K_a + [IMP]) \quad (1)$$

$$v = V_m[NAD^+]/(K_b + [NAD^+] + [NAD^+]^2/K_{ii}) \quad (2)$$

where v is the initial velocity, V_m is the maximal velocity, K_a and K_b are the Michaelis constants of IMP and NAD^+, respectively, and K_{ii} is the substrate inhibition constant for NAD^+. Steady-state parameters with respect to NAD^+ were derived by first determining the apparent values of V_m for the initial velocity versus IMP plots (eq 1) and replotting these values against NAD^+ concentration (eq 2). Similarly, the K_m value of IMP was derived by first determining the apparent values of V_m for the initial velocity versus NAD^+ concentration plots using eq 2 and replotting these values against IMP concentration (eq 1). No substrate inhibition is observed with APAD. Therefore, data were fit to a sequential mechanism (eq 3) using KinetAsyst software (Intellikinetics):

$$v = V_m[IMP][APAD]/(K_{ia}K_b + K_a[APAD] + K_b[IMP] + [IMP][APAD]) \quad (3)$$

where v is the initial velocity, V_m is the maximal velocity, K_a and K_b are the Michaelis constants of IMP and APAD, respectively, and K_{ia} is the dissociation constant of E·IMP. Primary deuterium isotope effects were measured using the substrate [2-^{2}H]IMP and determined by comparing the values of V_m and V/K_m for NAD^+, IMP, and APAD substrates in the fit of the data to eqs 1−3 as applicable.

Pre-steady-state experiments were performed on an Applied Photophysics SX.17MV stopped flow spectrophotometer at 25 °C. The production of NADH was monitored either by fluorescence (excitation wavelength of 340 nm, 420 nm cutoff emission filter) or by absorbance at 340 nm. Similarly, the production of APADH was monitored by fluorescence (excitation wavelength of 362 nm, 450 nm cutoff emission filter) or by absorbance at 363 nm. Enzyme and substrates were diluted 2-fold in assay buffer. Concentrations indicated in the text or figure legends are the final concentrations after dilution. The time course of fluorescence or absorbance can be described by a single-exponential equation with a steady-state term (eq 4):

$$S_t = (\Delta A)e^{-k_{obs}t} + vt \quad (4)$$

where S_t is the signal (fluorescence or absorbance) at time t, ΔA is the amplitude of the burst, k_{obs} is the observed first-order rate constant governing the burst phase, and v is the linear rate of increase in fluorescence or absorbance during the steady state. The data were analyzed by simulation of the time courses using the KINSIM program (*28*).

Equilibrium Dissociation Constants (K_d). Dissociation constants for the interaction of ligands with enzyme were determined by following the quenching of intrinsic protein fluorescence. The measurements were performed on a Hitachi F-2000 fluorescence spectrophotometer at 25 °C. The excitation wavelengths were 295 nm for NAD^+ and NADH and 280 nm for all other ligands. Inner filter effects due to the ligands were corrrected by the formula (*29*)

$$F_c = F_{obs}\ \text{antilog}[(A_{ex} + A_{em})/2] \quad (5)$$

where A_{ex} and A_{em} are the absorbances at the excitation and emission wavelengths, respectively, F_c is the corrected intensity, and F_{obs} is the measured intensity. The experiments involved successive titration of the apoenzyme solution with ligands. From the measured fluorescence intensity I at a given ligand concentration, the fractional saturation of enzyme sites with ligand (f_a) was determined by using $f_a = (I - I_a)/(I_b - I_a)$, where I_a is the fluorescence of the apoenzyme and I_b is the fluorescence of the enyzme when all of its binding sites are saturated with ligand. The free ligand concentration was estimated using $[ligand]_{free} = [ligand]_t - n[E]_t$, in which $[ligand]_t$ and $[E]_t$ represent the total ligand and apoenzyme concentrations, respectively, and n is the number of ligand binding sites on the enzyme ($n = 1$ for monomer concentration). Kaleidagraph software was used to fit f_a and $[ligand]_{free}$ to eq 6:

$$f_a = [L]_{free}/(K_d + [L]_{free}) \quad (6)$$

to give the dissociation constant K_d. When NAD^+ was the ligand, f_a and $[NAD^+]_{free}$ were fit to the Adair−Klotz equation (eq 7):

$$f_a = ([L]_{free}/K_1) + (2[L]_{free}^2/K_1K_2)]/[1 + ([L]_{free}/K_1) + ([L]_{free}^2/K_1K_2)] \quad (7)$$

to give the dissociation constants K_1 and K_2.

Table 1: Michaelis−Menten Parameters for *T. foetus* IMPDH[a]

dinucleotide substrate	NAD^+ [c]	APAD	NAD^+_{calc} [d]
$E^{\circ\prime}$ [b] (V)	−0.320	−0.258	−0.320
IMP K_m (μM)	1.7 ± 0.4	5.3 ± 1.4	2.1 ± 0.2
dinucleotide K_m (μM)	150 ± 30	450 ± 160	230 ± 10
dinucleotide K_{ii} (μM)	6800 ± 1800	na	7360 ± 390
k_{cat} (s^{-1})	1.9 ± 0.2	3.8 ± 0.3	1.7 ± 0.07
IMP V/K_m (M^{-1} s^{-1})	(1.1 ± 0.3) × 10^6	(7.2 ± 1.4) × 10^5	(0.8 ± 0.09) × 10^6
dinucleotide V/K_m (M^{-1} s^{-1})	(1.3 ± 0.3) × 10^4	(8.5 ± 2.7) × 10^3	(7.5 ± 0.2) × 10^3

[a] Reactions were performed in 100 mM KCl, 50 mM Tris (pH 8.0), 1 mM DTT, and 3 mM EDTA at 25 °C. Absorbance was monitored as described in Materials and Methods. na, not applicable. [b] $E^{\circ\prime}$ is the standard oxidation−reduction potential (pH 7, 25 °C). These values are from ref *44*. [c] Measured steady-state parameters. [d] Predicted steady-state parameters determined by generating initial velocities using KINSIM and fitting the data to eqs 1 and 2 in the text.

Kinetic Dissociation Constants. The individual rate constants for ligand binding were determined by stopped flow fluorescence spectroscopy at 25 °C. An excitation wavelength of 280 nm and emission wavelengths of >320 nm were used for fluorescence measurements of IMP, XMP, and GMP binding. Emission wavelengths between 298 and 435 nm were used for fluorescence measurements of NAD^+ and NADH binding. Enzymes and ligands were diluted 2-fold in assay buffer. The concentrations indicated in the text or figure legends are the final concentrations after dilution. The experiments were performed under pseudo-first-order conditions ([S] ≫ [E]), and the time course of fluorescence decrease at each concentration of ligand was fit to a single-exponential equation:

$$F_t = (\Delta F)e^{-k_{obs}t} + F_{eq} \quad (8)$$

where F_t is the fluorescence at time t, ΔF is the amplitude of the fluorescence decrease, k_{obs} is an apparent first-order rate constant, and F_{eq} is the fluorescence at equilibrium.

Labeling IMPDH with [^{14}C]IMP. The time course of labeling of enzyme with [^{14}C]IMP was determined by performing a chemical quench flow experiment using a RQF-3 Quench-Flow rapid mixer apparatus (KinTek). Reaction mixtures contained 4.5 μM IMPDH pre-incubated with 50 μM [^{14}C]IMP, and mixed with 0.8 mM NAD^+ in assay buffer at 25 °C. Reactions were allowed to proceed for different times (5 ms to 1.5 s) and were stopped by mixing with a quench solution (0.75−0.9 N HCl). The enzyme samples were then precipitated with 10% TCA and collected on 0.45 μm HA nitrocellulose filters (Millipore). A pulse-chase experiment was also performed in the quench flow apparatus using the same concentrations of reagents described above. The enzyme was first mixed with [^{14}C]IMP and NAD^+ for 1.5 s and then mixed with an excess of unlabeled IMP (4 mM). The reactions were stopped by the addition of 10% TCA and treated in the same fashion as described above. Control reactions in which NAD^+ was omitted from the assay mixture were performed for each experiment.

RESULTS AND DISCUSSION

Steady-State Kinetics. Michaelis−Menten parameters for *T. foetus* IMPDH are shown in Table 1. High concentrations of NAD^+ inhibit IMPDH. NAD^+ inhibition is uncompetitive, which is consistent with NAD^+ binding to E−XMP* as previously proposed for human IMPDH (*24*, *25*). Such behavior implies that product release is ordered, with NADH released first (*30*). The value of K_{ii} for NAD^+ is 45-fold greater than the value of K_m. The NAD^+ analog APAD is also a substrate for the enzyme. The value of K_m for APAD is 3-fold greater than that of NAD^+. The value of K_m for IMP with APAD as a substrate is also 3-fold greater than that measured with NAD^+ as a substrate. However, no substrate inhibition is observed for APAD. The value of k_{cat} is 3.8 s^{-1} with APAD, which is greater than that of NAD^+ by approximately 2-fold. Experiments were also performed with two other NAD^+ analogs, 3-pyridinealdehyde-NAD ($E^{\circ\prime}$ = −0.262) and nicotinamide hypoxanthine dinucleotide ($E^{\circ\prime}$ = −0.320) (data not shown). The k_{cat} values for these analogs are 2.4 and 2.6 s^{-1}, respectively. Despite the great differences in the structures and reduction potentials of these NAD^+ analogs, the values of k_{cat} are similar. This observation suggests that a common step is rate-limiting in these reactions, such as hydrolysis of E−XMP* or release of E·XMP. Thus, 3.8 s^{-1} is the lower limit for the common steps in the NAD^+ and APAD reactions.

Primary Deuterium Isotope Effects. No V_m isotope effect is observed when [2-^{2}H]IMP is the substrate (^DV = 1.1 ± 0.1), which indicates that hydride transfer is not rate-limiting for this dinucleotide. Isotope effects for $^D(V/K_m)$ were determined to be 0.5 ± 0.2 for IMP as the varied substrate and 2.0 ± 0.5 for NAD^+ as the varied substrate. Although the isotope effect for V_m is well-determined, relatively large errors are present in the $^D(V/K_m)$ data. A large inverse isotope effect appears to be observed on V/K_{IMP}. Since the value of K_m is so low (Table 1) and we are unable to assay at [IMP] ≪ K_m, this error is unavoidable. Therefore, we do not have confidence in the $^D(V/K_{IMP})$. We were unable to verify the inverse isotope effect in the pre-steady-state experiment (see below). Thus, we believe that $^D(V/K_{IMP})$ is close to 1. A significant isotope effect on V/K_{NAD} is observed. Since we were able to verify this isotope effect in the pre-steady-state experiment (see below), we have confidence in this value. The difference between $^D(V/K_{NAD})$ and $^D(V/K_{IMP})$ suggests that IMP is the "stickier" substrate (*31*). Similar isotope effects are observed when APAD is used as the substrate [^DV = 0.9 ± 0.1, $^D(V/K_{IMP})$ = 0.7 ± 0.2, and $^D(V/K_{APAD})$ = 2.4 ± 0.7].

Thermodynamics of Ligand Binding. The binding of IMP to IMPDH quenches the intrinsic protein fluorescence of the enzyme (Figure 2A). The value of the dissociation constant (K_d) for IMP binding can be determined from the dependence of fluorescence intensity upon substrate concentration (Table 2). Figure 2B shows a binding curve in which the changes in fluorescence are represented by fractional saturation of enzyme sites with IMP as its concentration increases.

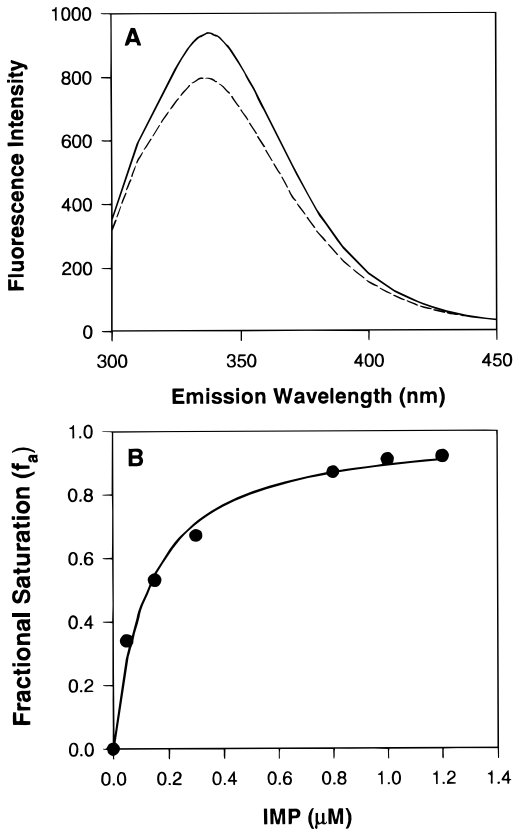

FIGURE 2: Binding of IMP to IMPDH. (A) Fluorescence emission spectra for IMPDH (solid line) and its complex with IMP (dashed line) when excited with light of 280 nm; the enzyme concentration is 0.2 μM, and the IMP concentration here is 1.0 μM. (B) Dependence of fractional saturation of the enzyme on IMP concentration as IMPDH is titrated with ligand. The data were fit to eq 6.

The binding curve is hyperbolic; therefore, there is no evidence of cooperativity for IMP binding to IMPDH. IMP was also shown to bind noncooperatively to the human type II IMPDH (*15*). However, isothermal titration calorimetry experiments performed with Chinese hamster IMPDH indicate that IMP binds to IMPDH with negative cooperativity (*32*).

GMP and XMP also bind to the free enzyme, with K_d values 10−20-fold higher than that of IMP (Table 2). The binding curves for these IMP analogs are also hyperbolic (data not shown). XMP was also shown bind to human IMPDH in a noncooperative fashion (*15*).

NADH and NAD^+ also quench the enzyme fluorescence (data not shown). As with the IMP analogs, the binding curve for NADH is hyperbolic. NADH also binds to human IMPDH noncooperatively (*15*). Interestingly, the binding curve for NAD^+ is sigmoidal (not shown) and is best fit to the Adair−Klotz equation (eq 7) with $n = 2$ to give two dissociation constants: $K_1 = 340$ μM and $K_2 = 1600$ μM ($\bar{K} = 740$ μM). These data imply that NAD^+ exhibits cooperativity when binding to the enzyme. Alternatively, the binding of NAD^+ to each subunit could display a nonidentical fluorescence decrease. We cannot distinguish between these two possibilities. However, since no cooperativity is observed either for NADH binding or in the steady-state kinetics, we favor the latter explanation. In studies of human type II IMPDH and Chinese hamster IMPDH, binding of NAD^+ to the free enzyme could not be detected (*15*, *16*). Therefore, this is the first demonstration of NAD^+ binding to free IMPDH. The fact that both substrates bind to the free enzyme is consistent with a random addition of substrates for *T. foetus* IMPDH.

MPA also quenches the fluorescence of the enzyme−IMP complex (data not shown). As with the other ligands, the binding curve is hyperbolic. Using eq 6, a K_d of 110 μM was determined for the binding of MPA to the IMPDH−IMP complex.

Kinetics of Ligand Binding: IMP Binds in Two Steps. When IMP is mixed with enzyme, the fluorescence intensity rapidly decreases with time. Figure 3A shows results from a representative experiment. The data were fit to eq 8 to obtain values of k_{obs} at each ligand concentration. The linear dependence of k_{obs} on IMP is shown in Figure 3B, and eq 9 can be used to extract the values of k_1 and k_{-1} (*33*).

$$k_{obs} = k_1[S] + k_{-1} \quad (9)$$

Here, k_1 and k_{-1} are association (k_1) and dissociation (k_{-1}) rate constants governing ligand binding, respectively. The values of k_1 and k_{-1} calculated in this manner are shown in Table 2. The value of k_1 for IMP is similar to its k_{cat}/K_m value (Table 1). This linear dependence on ligand concentration suggests a simple bimolecular association binding, indicated by Scheme 1. However, the value of k_{-1}/k_1 should

Table 2: Kinetic and Thermodynamic Constants for Ligand Binding for Wild-Type and Cys319Ser IMPDHs[a]

ligand	k_1 ($\times 10^6$ M^{-1} s^{-1})	k_{-1} (s^{-1})	k_2 (s^{-1})	k_{-2} (s^{-1})	$K_{d(calc)}$ (μM)	K_d[d] (μM)
			wild-type			
IMP[e]	2.6	7.7	21	1.1	na	0.15
XMP[f]	6.7	17	−	−	2.5[b]	3.9
GMP[g]	≥21	−	200	21	1.0[c]	2.0
NAD^+[f]	0.043	41	−	−	950[b]	740[h]
NADH[f]	0.64	6.7	−	−	10.5[b]	15.7
			Cys319Ser			
IMP[e]	2.8	27	0.6	1.1	na	6.2
XMP[f]	8.5	10.5	−	−	1.2[b]	3.0
NAD^+[f]	0.24	65	−	−	270[b]	615

[a] Binding assays were performed in 100 mM KCl, 50 mM Tris (pH 8.0), 1 mM DTT, and 3 mM EDTA at 25 °C. na, not applicable. The standard deviation of all parameter values is ≤20%. [b] Calculated from k_{-1}/k_1. [c] Calculated from $(K_1k_{-2})/(k_2 + k_{-2})$, where K_1 is the apparent dissociation constant for the first step. [d] Thermodynamic dissociation constant for the formation of the binary complex determined by ligand titration and monitoring the accompanying fluorescence decrease. [e] Two-step binding, where k_{-2} was determined by ligand exchange and k_2 was determined by eq 10. [f] One-step binding. [g] Two-step binding, in which the first step is in rapid equilibrium. Values of k_{-2} and k_2 were determined by eq 11. [h] The sigmoidal binding curve for NAD^+ gives two binding constants, K_1 and K_2, with an overall $\bar{K}$ of $(K_1K_2)^{1/2}$.

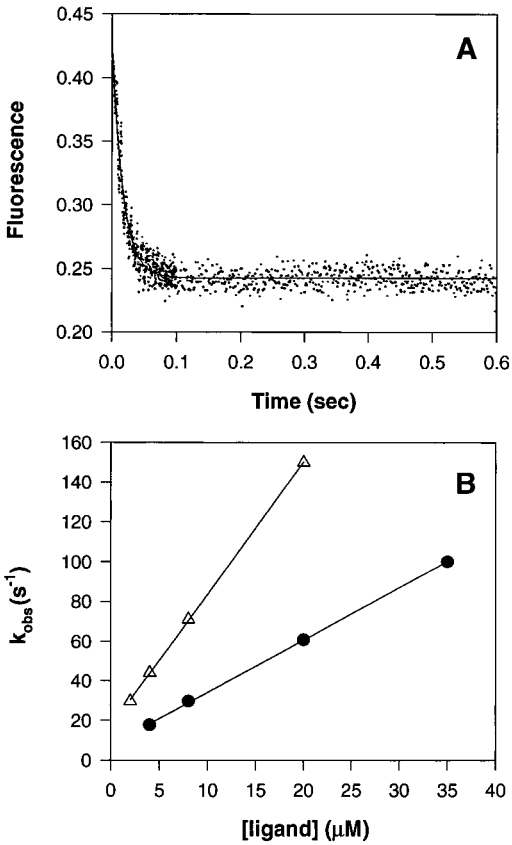

FIGURE 3: Kinetics of IMP and XMP binding to IMPDH. (A) Time course of IMP association with IMPDH. The concentration of IMPDH is 0.8 μM, and that of IMP is 20 μM. The enzyme was excited with light of 280 nm, and emission was monitored with a 320 nm cutoff filter. The line represents the best fit of the data to eq 8. (B) Dependence of k_{obs} on (●) IMP and (△) XMP concentration.

Scheme 1: One-Step Binding

$$E + S \underset{k_{-1}}{\overset{k_1[S]}{\rightleftharpoons}} E \cdot S$$

Scheme 2: Ligand Exchange Experiment

$$E \cdot IMP \xrightarrow{k_{off}} E + IMP \qquad E \underset{k_{-2}}{\overset{k_2[XMP]}{\rightleftharpoons}} E \cdot XMP$$

be equal to the thermodynamically measured value of K_d if Scheme 1 is valid. Surprisingly, the value of k_{-1}/k_1 (3.0 μM) is 20-fold higher than the thermodynamic dissociation constant (0.15 μM). Thus, there is another step of binding which is not monitored in this experiment. This second step could easily have been missed during the stopped flow experiment if it was not fluorescence sensitive.

To elucidate another step of IMP binding, a ligand exchange experiment was performed. IMP is displaced with XMP under conditions in which the rate-limiting step is the release of the bound IMP (*33*). The experimental setup is described in Scheme 2. The experiment follows the appearance of E·XMP. Conditions were chosen so that IMP dissociation is irreversible and XMP association is fast. Figure 4 shows a trace for the displacement of IMP from the enzyme by an excess of XMP. The reaction is described by a single exponential with a k_{off} value of 1.1 ± 0.06 s^{-1} at

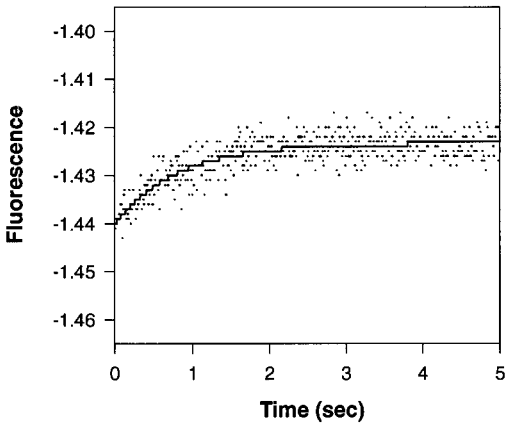

FIGURE 4: Ligand exchange experiment, with measurement of the dissociation rate constant for IMP. Time course of fluorescence change when E·IMP is mixed with XMP, forming E·XMP. Final concentrations are as follows: 0.5 μM IMPDH, 10 μM IMP, and 200 μM XMP. The enzyme was excited with light of 280 nm, and the emission was monitored with a 320 nm cutoff filter. The time course was monitored for 10 s, and the first 5 s is shown here. The line represents the fit of the data to a single-exponential equation.

Scheme 3: Two-Step Binding

$$E + IMP \underset{k_{-1}}{\overset{k_1[S]}{\rightleftharpoons}} E \cdot IMP \underset{k_{-2}}{\overset{k_2}{\rightleftharpoons}} E' \cdot IMP$$

an XMP concentration of 200 μM. A similar value of k_{off} (0.93 ± 0.15 s^{-1}) was obtained at an XMP concentration of 800 μM, demonstrating that the reaction is independent of XMP concentration. The average of these two numbers gives a value of 1.1 ± 0.18 s^{-1} for the k_{off} of IMP. This rate constant is smaller than that obtained in the ligand association experiment (7.7 s^{-1}), confirming that there is an isomerization step following the initial formation of the E·IMP complex, as depicted in Scheme 3. By using eq 10 (*34*), k_2 can be determined:

$$K_d = K_1[k_{-2}/(k_2 + k_{-2})] \qquad (10)$$

Here, K_d is the thermodynamic dissociation constant, $K_1 = k_{-1}/k_1$ was determined previously, and k_{-2} is the k_{off} determined by ligand exchange. The rate constant k_2 was calculated to be 21 ± 4 s^{-1}.

Binding of IMP Analogs. When XMP is mixed with IMPDH, the observed fluorescence intensity decreases with time (data not shown). The linear dependence of k_{obs} on ligand concentration is shown in Figure 3B, and the values for the association and dissociation rate constants were determined as described above for IMP binding. As can be seen in Table 2, the value of k_{-1}/k_1 is similar to the K_d value. Therefore, XMP binds to the enzyme in a simple bimolecular association as indicated in Scheme 1.

When GMP binds to IMPDH, the observed fluorescence intensity rapidly decreases with time. Unlike those of the other ligands, the observed first-order rate constant shows a hyperbolic dependence on GMP concentration (data not shown). The data were fit to eq 11, which describes a two-step binding mechanism in which the first step is in rapid equilibrium (*33*).

$$k_{obs} = [k_2[GMP]/([GMP] + K_1)] + k_{-2} \qquad (11)$$

From this analysis, values of K_1, k_2, and k_{-2} were determined to be 9.5 μM, 200 s^{-1}, and 21 s^{-1}, respectively. A lower limit for the apparent second-order rate constant, k_1 (Table 2), is Kk_2, where $K = 1/K_1$. The dissociation constant for GMP is given by $(K_1k_{-2})/(k_2 + k_{-2})$ (=1.0 μM), which is in agreement with the thermodynamic value of 2.0 μM.

Binding of Dinucleotides. NAD^+ and NADH also bind to the enzyme, causing the fluorescence intensity to decrease with time. The dependence of k_{obs} on both ligand concentrations is linear (data not shown), and the association and dissociation rate constants were determined by eq 9 (Table 2). The value of k_1 for NAD^+ is similar to its k_{cat}/K_m value (Table 1). Since the values of k_{-1}/k_1 are similar to the values of K_d, the binding of both ligands to the enzyme occurs by a simple, one-step mechanism.

Investigation of the Isomerization Step during IMP Binding: The Cys319Ser Mutant. The nature of the isomerization during IMP binding is not currently known, but two postulates exist. It could be a conformational change, such as flap movement over the active site. Such a conformational change is well precedented in enzymatic reactions (*35*), and a conformational change upon IMP binding to Chinese hamster IMPDH has been proposed by others (*16*, *32*). The isomerization could also be the covalent addition of the active site Cys319 to the C-2 of IMP to form E−IMP (Figure 1).

To investigate the nature of the isomerization, a mutant was constructed in which Cys319 was mutated to Ser. Model studies have shown that thiols are more potent nucleophiles than hydroxyls in several nucleophilic displacement reactions (*36*). Thus, serine is unlikely to form a covalent adduct with IMP. The mutant enzyme has less than 0.06% of the wild-type activity. Binding of IMP, XMP, and NAD^+ to the mutant enzyme quenches the intrinsic protein fluorescence (data not shown). Values of the kinetic and thermodynamic dissociation constants were determined in the same manner as those of the wild type and are shown in Table 2. XMP and NAD^+ bind to the mutant enzyme with K_d values similar to wild-type values. Therefore, binding of these ligands is not affected by the mutation. However, NAD^+ binding to Cys319Ser displays a hyperbolic binding curve (data not shown), which differs from the sigmoidal binding curve for NAD^+ binding to wild-type IMPDH. For IMP, the value of K_d is 40-fold higher than that for the wild type. Here, the value of k_{-1}/k_1 (9.6 μM) is very close to the value of K_d (6.2 μM).

To determine if the isomerization step was still present, the ligand exchange experiment was performed, again using XMP as the competing ligand (Figure 5). The dashed line shows a simulation representing a one-step dissociation of IMP from the enzyme with a k_{off} of 27 s^{-1}. The simulation does not correlate with the actual data. The data were best fit to a double-exponential equation, giving two rate constants, 21 ± 5 and 1.1 ± 0.1 s^{-1}. The first rate constant is similar to that measured with the relaxation technique (27 s^{-1}). However, 1.1 s^{-1} is slower than 27 s^{-1}. Therefore, these data are consistent with an isomerization following association of IMP with the enzyme with a k_{-2} of 1.1 s^{-1} (Scheme 3 and Table 2). Using eq 10, the rate constant k_2 was calculated to be 0.6 s^{-1}. This rate constant for isomerization is much slower than the value of k_2 for the wild type (21 s^{-1}). The isomerization step for the mutant has an equilibrium of about 1; therefore, it is expected that the amplitudes of both phases should be equal in the ligand exchange experiment. As predicted, the values of the amplitudes are $(9.0 \pm 1.2) \times 10^{-3}$ and $1.1 \times 10^{-2} \pm 5.8 \times 10^{-4}$.

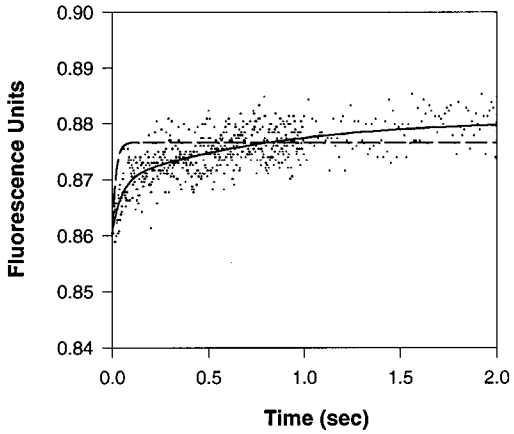

FIGURE 5: Ligand exchange experiment, with measurement of the dissociation rate constant for the Cys319Ser E·IMP complex. Time course of fluorescence change when E·IMP is mixed with XMP, forming E·XMP. Concentrations are as follows: 0.5 μM IMPDH, 30 μM IMP, and 100 μM XMP. The enzyme was excited with light of 280 nm, and the emission was monitored with a 320 nm cutoff filter. The time course was monitored for 5 s, and the first second is shown here. The solid line represents the fit of the data to a double-exponential equation. The dashed line represents a simulation of a one-step dissociation of IMP from the enzyme using KINSIM.

These results suggest that IMP binds to Cys319Ser in a two-step mechanism as observed with wild-type IMPDH, although the affinity of IMP is reduced by 40-fold. The decrease in affinity is derived from a decrease in k_2. While this decrease is substantial, it is less than would be expected if k_2 represented nucleophillic addition of Cys319 to IMP for the following reasons. (1) Bronsted analysis of thiol and alcohol nucleophiles suggests that a cysteine residue will be 1000 times more nucleophilic than a serine (*37*, *38*).[2] (2) Substitutions of cysteine nucleophiles with serine in other enzymes are consistent this estimate (*39*−*42*), although as yet a quantitative comparison of cysteine and serine nucleophiles for these enzymes is not available. (3) While wild-type IMPDH reacts instantaneously with EICARMP as detected by UV spectroscopy, forming an adduct with Cys319 (*21*), we failed to detect the formation of an adduct between Cys319Ser and EICARMP after 10 min (data not shown). This would suggest that Ser319 is at least 600-fold less reactive than Cys319.

Therefore, it is likely that k_2 represents a conformational rearrangement of the enzyme rather than addition of Cys319 to IMP. The loop containing Cys319 (residues 314−324) is disordered in the absence of substrates (*20*). This loop appears to contribute residues to both the IMP and NAD^+ binding sites (*19*), and would be expected to become ordered upon IMP binding. It is possible that k_2 represents the

[2] If normal values of pK_a are assumed for serine and cysteine residues at position 319, their reactivity can be estimated from Bronsted analysis of the reaction of anionic sulfur and oxygen nucleophiles with *p*-nitrophenyl acetate (*37*, *38*). The reactivity of an alkoxide nucleophile with a pK_a of 14.2 is ~100 times greater than that of a thiolate nucleophile with a pK_a of 8.7. However, at pH 8, there will be ~10^5-fold more thiolate than alkoxide. Therefore, at pH 8, Cys319 is expected to be 1000-fold more reactive than Ser319.

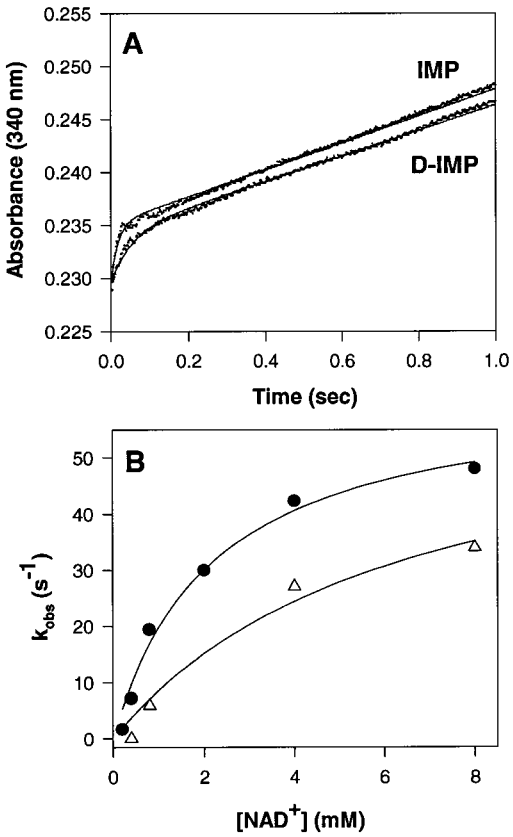

FIGURE 6: Pre-steady-state burst of NADH (or NADD) production, as determined with absorbance. (A) The top trace shows the approach to the steady-state rate obtained when 2.0 μM enzyme was preincubated with 50 μM IMP and mixed with 8 mM NAD^+ under assay conditions (see Materials and Methods). The bottom trace shows the same conditions using [2-^{2}H]IMP. The time courses were monitored for 2 s, and shown here is the first second of the reactions. The lines are the fits of the data to eq 4 in the text. (B) Dependence of k_{obs} on NAD^+ concentration. Rate constants for burst formation vs NAD^+ concentration with (●) IMP as a substrate and (△) [2-^{2}H]IMP as a substrate. The data were fit to eq 12 to obtain values of k_{burst} for both substrates.

ordering of this loop. Further, this loop remains disordered in the E·XMP complex (*20*), which is consistent with the failure to observe the isomerization step when XMP binds to IMPDH. Since Cys319 must be close to IMP, it seems reasonable to expect that the serine substitution will also perturb this conformational change.

Determination of the Binding Rate Constants of the Binary Complexes. Because Cys319Ser has negligible activity, it was possible to measure association and dissociation rate constants for IMP binding to enzyme saturated with NAD^+. The k_{on} measured in this way was 2.2×10^6 M^{-1} s^{-1}, and k_{off} = 4.7 s^{-1}. Similarly, the association and dissociation rate constants for NAD^+ binding to enzyme saturated with IMP were found to be 2.0×10^5 M^{-1} s^{-1} and 94 s^{-1}, respectively.

Pre-Steady-State Kinetics Measured by Absorbance. The steady-state isotope effect experiment indicates that hydride transfer is not rate-determining. This observation is confirmed by the presence of a pre-steady-state burst of NADH production measured by an increase in absorbance at 340 nm. Enzyme was preincubated with saturating IMP and mixed with NAD^+ (Figure 6A), and the data were fit to a single-exponential equation with a steady-state term (eq 4). As shown in Figure 6B, the rate constants for the exponential phase, k_{obs}, display a hyperbolic dependence on NAD^+ concentration. The maximum value of k_{obs}, denoted k_{burst}, was calculated according to eq 12 and is shown in Table 3:

$$k_{obs} = k_{burst}[NAD^+]/(K_{app} + [NAD^+]) \qquad (12)$$

where K_{app} is the concentration of varied substrate at one-half of the maximum value of k_{burst}. The concentrations of NAD^+ used for the pre-steady-state experiments are inhibitory under steady-state conditions. The presence of a burst at these concentrations indicates that NAD^+ does not inhibit IMPDH in the first turnover, and is consistent with the formation of an E−XMP*·NAD^+ inhibitory complex. A primary isotope effect equal to 1.4 is observed on k_{burst} when starting with E·IMP. This observation implies that the value of k_{burst} represents the hydride transfer step. However, since this number is small for an intrinsic isotope effect, this rate constant could also include another step. The value of $^D(k_{burst}/K_{app})$ of 2.2 agrees with the $^D(V/K_{NAD})$ value determined from the steady-state kinetic experiment (2.0).

Table 3: Pre-Steady-State Kinetics Monitored by Absorbance and Isotope Effects[a]

beginning complex	varied substrate	k_{burst}[b] (s^{-1})	$^Dk_{burst}$	$^Dk_{burst}/K_{app}$	[NADH]/[E]$_t$[e]
E·IMP	NAD^+	62 ± 6	1.4 ± 0.2	2.2 ± 0.3	0.45 ± 0.01
E·NAD^+	IMP	22 ± 3	1.9 ± 0.2	1.5 ± 0.5	0.56 ± 0.02
E	IMP, NAD^+[c]	31 ± 6	−	−	0.55 ± 0.06
E·IMP	APAD	≥415[d]	−	−	0.80 ± 0.10

[a] The time course of absorbance can be described by a single-exponential equation with a steady-state term. The rate constant for the exponential phase is k_{obs}. [b] The rate constants for k_{obs} display a hyperbolic dependence on NAD^+ and IMP concentrations. Using eq 12 in the text, the maximum value, k_{burst}, can be determined. [c] The IMP concentration is saturating, and the NAD^+ concentration varies. [d] The rate constant for the exponential phase is linearly dependent on APAD concentration up to concentrations of 8 mM (k_{obs} = 208 s^{-1}). This concentration of APAD is approximately one-half of the K_{app} (eq 12). [e] The NADH concentration is obtained from $\Delta A_{340}/\epsilon l$, where ΔA_{340} is the amplitude of the burst, ϵ is 6.22 mM^{-1} cm^{-1} for NADH and 9.1 mM^{-1} cm^{-1} for APADH, and l is the path length (1 cm).

As can be seen in Table 3, the amplitude of the burst is about one-half of the enzyme concentration ([NADH]/[E]$_t$ = 0.45 ± 0.01). This observation can be explained in two ways. Since the enzyme is a tetramer, it could be using only two of its active sites, a phenomenon known as half-site reactivity. However, several lines of evidence suggest that all of the active sites are operational in IMPDHs from other sources: (a) one IMP is bound per active site in human IMPDH (*15*); (b) all of the active sites of *E. coli* IMPDH are modified by affinity agents (*21*); and (c) one molecule of NADH is produced per active site of mammalian IMPDHs in the presence of MPA (*11*, *26*). Another possibility is that NADH release could be slow, allowing an equilibrium to form at the hydride transfer step. To distinguish between these two possibilities, APAD was used as a substrate. Since its reduction potential is higher than that of NAD^+ (Table 1), the position of the equilibrium of the hydride transfer step will shift toward products. However, if the enzyme is using only two of its active sites, the amplitude will remain 0.5. As can be seen is Table 3, the amplitude of the burst is now 0.80 ± 0.10 in the presence of APAD. Therefore, half-site reactivity can be ruled out as a possible explanation.

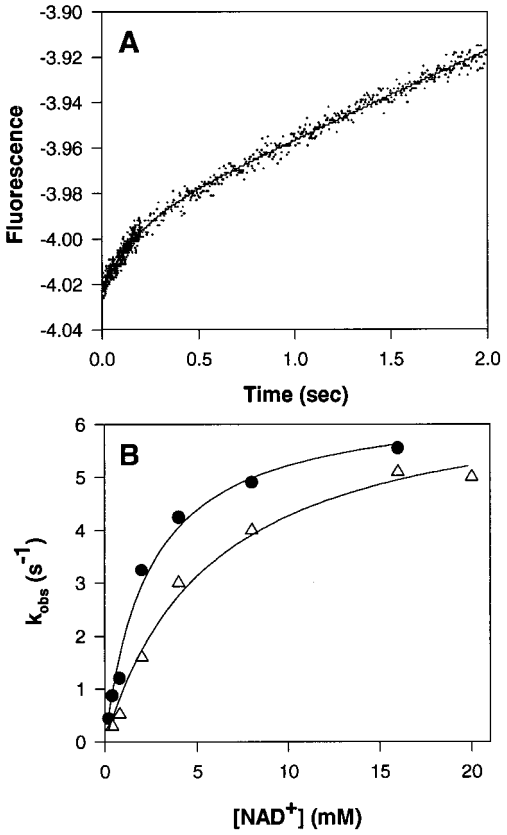

FIGURE 7: Pre-steady-state burst of NADH production, as determined with fluorescence. (A) This trace shows the approach to the steady-state rate obtained when 0.5 μM enzyme was preincubated with 50 μM IMP and mixed with 16 mM NAD^+ under assay conditions. The line represents the fit of the data to eq 4 in the text. (B) Dependence of k_{obs} on NAD^+ concentration. Rate constants for burst formation vs NAD^+ concentration with (●) IMP as a substrate and (△) [2-^{2}H]IMP as a substrate. The data were fit to eq 12 to obtain values of k_{fluor} for both substrates.

This result suggests that the NADH release step is slow enough to allow the hydride transfer step to be at equilibrium.

Similar data were obtained when the enzyme was preincubated with NAD^+ and mixed with IMP (Table 3). A burst of NADH formation is observed with an amplitude of ~0.5. A primary isotope effect equal to 1.9 is observed. This isotope effect is also too small to be intrinsic, implying that the k_{burst} could be a combination of hydride transfer and some other step. This step could be a conformational change similar to that observed upon IMP binding to unliganded enzyme. The value of $^D(k_{burst}/K_{app})$ for IMP is 1.5, which does not agree with the $^D(V/K_{IMP})$ observed in the steady-state experiment. As discussed above, we believe that 1.5 is a more accurate determination.

When the apoenzyme is mixed with saturating IMP and varied NAD^+ concentrations, a burst of NADH production is also observed (data not shown). The data were handled as described above for the E·IMP complex and are shown in Table 3. The value of k_{burst} is 31 s^{-1}, which, within error, is the same rate as when starting with E·NAD^+. The amplitude data are also in agreement with previous results.

Pre-Steady-State Kinetics Measured by Fluorescence. The pre-steady-state kinetics were also determined by monitoring the production of NADH by fluorescence. Figure 7A shows the burst of NADH production when the enzyme is preincubated with IMP. As when absorbance is monitored, the rate constants for the exponential phase, k_{obs}, display a hyperbolic dependence on NAD^+ concentration (Figure 7B). The maximum value of k_{obs}, denoted k_{fluor}, was determined by eq 12 and found to be 6.5 s^{-1} (Table 4). Since this value is not much greater than the k_{cat} value (1.9 s^{-1}), the presence of a burst is somewhat surprising. However, the concentrations of NAD^+ used for these pre-steady-state experiments are inhibitory in the steady state. As noted above, NAD^+ does not inhibit in the first turnover. Therefore, the presence of the "burst" here is simply due to the NAD^+ inhibition occurring after the first turnover. Similar data were obtained when the enzyme was first preincubated with NAD^+ or when the apoenzyme was mixed with IMP and NAD^+ (Table 4).

Table 4: Pre-Steady-State Kinetics Monitored by Fluorescence and Isotope Effects[a]

beginning complex	varied substrate	k_{fluor}[b] (s^{-1})	$^Dk_{fluor}$	$^Dk_{fluor}/K_{app}$
E·IMP	NAD^+	6.5 ± 0.3	1.0 ± 0.1	2.3 ± 0.3
E·NAD^+	IMP	5.6 ± 0.3	–	–
E	IMP, NAD^+[c]	6.1 ± 0.6	–	–
E·IMP	APAD	≥60[d]	–	–

[a] The time course of fluorescence can be described by a single-exponential equation with a steady-state term. The rate constant for the exponential phase is k_{obs}. [b] The rate constants k_{obs} display a hyperbolic dependence on NAD^+ and IMP concentrations. Using eq 12 in the text, the maximum value, k_{fluor}, can be determined. [c] The IMP concentration is saturating, and the NAD^+ concentration varies. [d] The rate constant for the exponential phase is linearly dependent on APAD concentration up to concentrations of 20 mM (k_{obs} = 12 s^{-1}). This concentration of APAD is approximately one-fifth of the K_{app} (eq 12).

Interestingly, the values of k_{fluor} are 5−10-fold lower than k_{burst} (Tables 3 and 4). This observation indicates that the fluorescence and absorbance experiments are probing different steps of the mechanism. We propose that the fluorescence of enzyme-bound NADH in the ternary complex is quenched. Therefore, k_{fluor} measures NADH release. This proposal is based on similar results with the pig heart lactate dehydrogenase reaction, where the fluorescence of NADH is quenched in the enzyme−pyruvate−NADH complex (*43*). This hypothesis predicts (a) the value of k_{fluor} will not depend on the starting complex (E, E·IMP, or E·NAD^+) since NADH release is a common step for all three complexes and (b) no primary isotope effect will be observed since the hydride transfer is not monitored. Both of these predictions are fulfilled (Table 4). In addition, the value of k_{flour} is identical to the rate constant for release of NADH from E·NADH (6.5 and 6.7 s^{-1}, respectively; Tables 2 and 4). We also performed a fluorescence energy transfer experiment utilizing the tryptophans in the enzyme as the fluorescence donor and the NADH as the acceptor (excitation λ = 280 nm, emission $\lambda \geq$ 420 nm) (data not shown). We failed to observe energy transfer, which suggests that the fluorescence signal does not arise from enzyme-bound NADH. For these reasons, we assigned k_{fluor} to the NADH release step. Alternatively, k_{fluor} might represent a conformational change occurring after hydride transfer but prior to NADH release which unveils the fluorescence of NADH. However, we believe this prospect is unlikely in view of the energy transfer results. In either event, a slow step follows hydride transfer, which indicates that the hydride transfer step will be at equilibrium as postulated above.

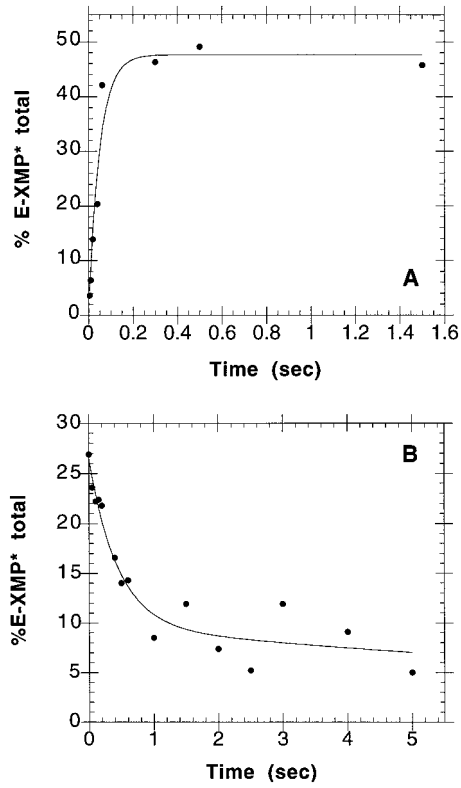

FIGURE 8: Rapid quench experiment, in which the steady-state level and decay of E−XMP* intermediates were assessed. Experimental conditions are described in Materials and Methods. (A) This figure shows the time course of formation and the steady state level of E−XMP* intermediates (E−XMP*, E−XMP*·NADH, and E−XMP*·NAD^+). The circles represent real data points, and the line represents a fit of the data to a single-exponential equation. (B) The decay of E−XMP* intermediates was monitored by performing a pulse-chase experiment. The circles represent real data points, and the line represents a fit of the data to a single-exponential equation.

The value of k_{fluor} when APAD is used as a substrate ($\geq$60 s^{-1}) is much greater than that measured with NAD^+ (6.5 s^{-1}). The value of k_{fluor} for APAD is greater than its k_{cat} (3.8 s^{-1}). If it is assumed that k_{fluor} represents APADH release, 3.8 s^{-1} can be assigned to a common step in both the NAD^+ and APAD reactions. Since the rate of XMP release is 17 s^{-1} (Table 2), this 3.8 s^{-1} step is most likely hydrolysis of E−XMP*. Since NADH release is faster than hydrolysis of E−XMP*, product release must be ordered, with NADH release preceding hydrolysis.

Rapid Quench Kinetics. The time course of formation of acid precipitable [^{14}C]E−XMP* was monitored by performing a chemical quench flow experiment. The enzyme was mixed with [^{14}C]IMP and NAD^+, and the reaction was stopped at various time points with a quench solution. Figure 8A shows the approach to the steady-state level of E−XMP* intermediates (E−XMP*, E−XMP*·NADH, and E−XMP*·NAD^+). The data were fit to a single-exponential equation, giving a k_{obs} of 20 $\pm$ 3 s^{-1}; this value is the same as the observed first-order rate constant governing the exponential phase for absorbance at the concentration of NAD^+ used in this experiment (0.8 mM NAD^+). These data confirm that hydride transfer is fast and subsequent steps are rate-limiting for the IMPDH reaction. The amplitude of 48 $\pm$ 3% also agrees with the amplitude from the pre-steady-state absorbance data. These results indicate that about 50% of the enzyme is in the E−XMP* complex.

A pulse-chase experiment was also performed to monitor the decay of [^{14}C]E−XMP* intermediates (Figure 8B). The enzyme was first mixed with [^{14}C]IMP and NAD^+ for 1.5 s to reach a steady-state level of E−XMP* and then mixed with an excess of unlabeled IMP at different time points. The interpretation of these data is a bit difficult since E−XMP*, E−XMP*·NADH, and E−XMP*·NAD^+ contribute to the signal. Since NAD^+ is present at 0.8 mM in this experiment and the K_{ii} = 6.8 mM, E−XMP*·NAD^+ can be ignored. Since NADH release and E−XMP* hydrolysis are comparable, with rate constants of 6.5 and 3.8 s^{-1}, respectively, the decay of E−XMP* intermediates is expected to be a double-exponential process. However, the data lack the precision and resolution necessary to detect a double-exponential process. The data were therefore fit to a single-exponential equation, giving a k_{obs} of 1.9 $\pm$ 0.4 s^{-1}, which is equal the k_{cat} value of 1.9 s^{-1}. These data are consistent with the rate constants for both NADH release and E−XMP* hydrolysis in the expression for k_{cat}: $(6.5 \times 3.8)/(6.5 + 3.8) = 2.4\ s^{-1}$.

Summary of the Overall Kinetic Scheme. We have combined the above data to construct an overall kinetic scheme for the IMPDH reaction (Scheme 4). All of the rate constants have been measured directly, except those for hydrolysis of E−XMP* and addition of NAD^+ as a substrate inhibitor to E−XMP*. The hydrolysis rate constant was determined from the k_{cat} of the APAD reaction, and the rate constants for NAD^+ as a substrate inhibitor were simulated, constrained by the value of K_{ii}. The rate constants for the two-step binding of IMP were determined from the ligand exchange experiment (Figure 4). The signal-to-noise ratio in this figure is quite low. However, using the outer confidence limits for the isomerization rate constants (k_2 and k_{-2}, Scheme 3) in the kinetic model does not affect the correlation of the simulation to actual data (see below). The rate constants for hydride transfer are derived from the stopped flow experiment with E·IMP as the starting complex. The ratio of forward and reverse hydride transfer was determined from the amplitude of the absorbance burst and the quench experiments. The main features of this mechanism are as follows. (1) Substrates bind in a random fashion. IMP binds to IMPDH in a two-step mechanism. The isomerization is most likely a conformational change of the enzyme. (2) Hydride transfer is fast and reversible, with an equilibrium of 1. (3) Product release appears to be ordered, with NADH release preceding hydrolysis of E−XMP*. (4) NADH release and hydrolysis of E−XMP* are both rate-limiting.

A good test of the validity of Scheme 4 is to determine if it will describe the time course of the IMPDH reaction. Figure 9A shows the time course for the reaction when the production of NADH was followed by absorbance at 340 nm, as measured by stopped flow spectroscopy. The solid line in this figure is based on data simulated by the computer program KINSIM using the rate constants in Scheme 4. The simulation output included both enzyme-bound and free NADH. Figure 9B shows the time course for the reaction when the production of NADH was followed by fluorescence. In this figure, the fluorescence units were normalized with absorbance units. The solid line in this figure is the simulation, again by KINSIM using the rate constants in Scheme 4. The simulation output for this trace included only

Scheme 4: Kinetic Scheme for *T. foetus* IMPDH

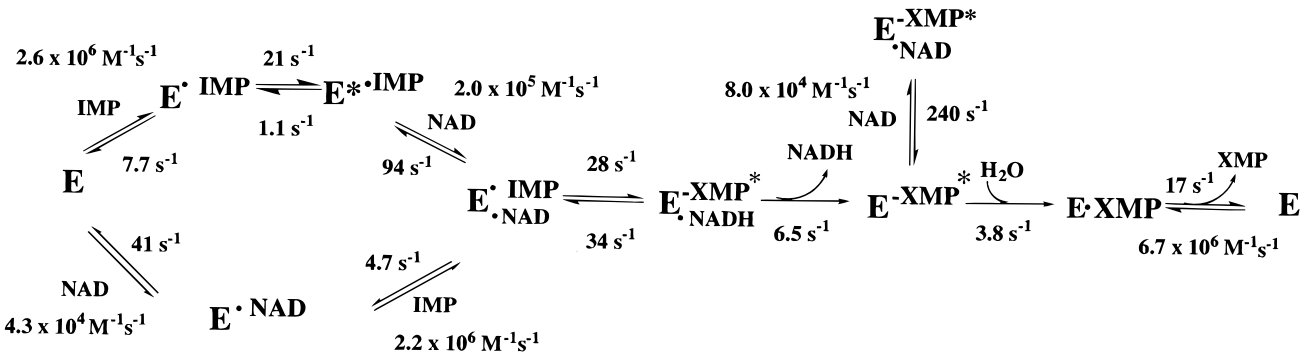

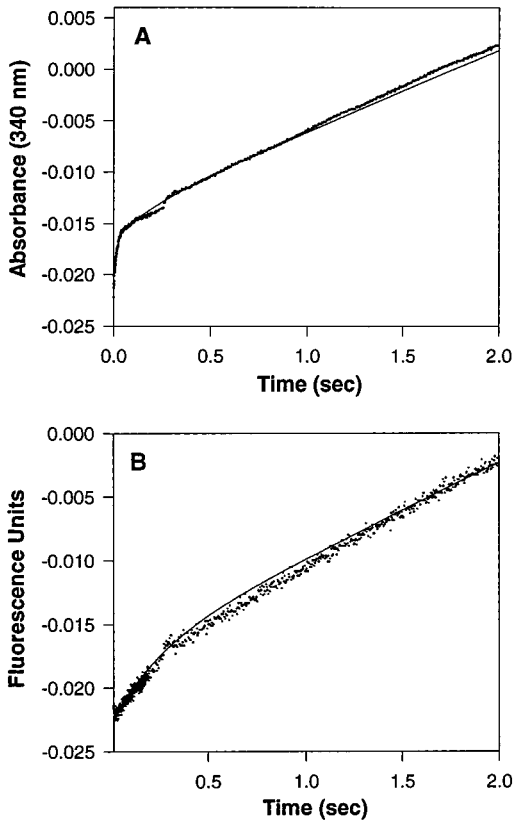

FIGURE 9: Simulations of the time course for the IMPDH reaction as measured by stopped flow absorbance and fluorescence. (A) This trace shows the approach to the steady-state rate obtained when 2.0 μM enzyme was preincubated with 50 μM IMP and mixed with 8 mM NAD^+ under assay conditions. The solid line for the time course was simulated with KINSIM using the kinetic model and rate constants in Scheme 4. The simulation output included both enzyme-bound and free NADH. (B) This trace shows the approach to the steady-state rate obtained when 0.5 μM enzyme was preincubated with 50 μM IMP and mixed with 8 mM NAD^+ under assay conditions. Production of NADH was monitored by fluorescence, and has been normalized with absorbance units here. The solid line for the time course was simulated with KINSIM using the kinetic model and rate constants in Scheme 4. The simulation output included only free NADH.

free NADH. As can be seen, the time course for the *T. foetus* IMPDH reaction can be predicted quite accurately using the measured rate constants.

A second test of the validity of Scheme 4 is to see if it correlates with the steady-state kinetics of *T. foetus* IMPDH. Steady-state parameters for the proposed model (Scheme 4) were determined by using KINSIM to calculate steady-state initial velocity data and fitting the data to eqs 1 and 2. The

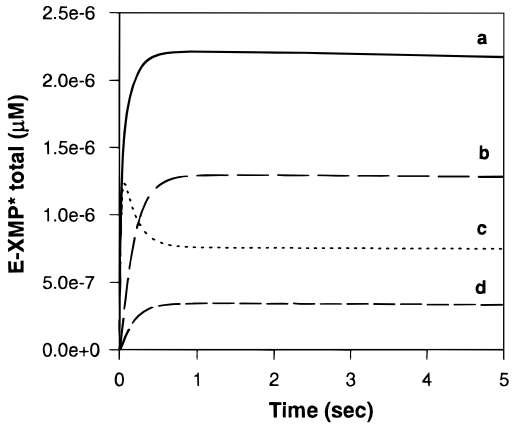

FIGURE 10: Simulation of the IMPDH reaction, in which steady-state levels of E−XMP* intermediates were determined. Shown here is a simulation of E−XMP* intermediates generated with KINSIM using the rate constants in Scheme 4: (a) E−XMP* and E−XMP*·NADH, (b) E−XMP*, (c) XMP*·NADH, and (d) E−XMP*·NAD^+.

predicted parameters determined in this manner are shown in Table 1. As can be seen, the agreement is quite good. Therefore, Scheme 4 is a valid model for the overall kinetic scheme of *T. foetus* IMPDH.

Figure 10 shows a simulation of the steady-state levels of the E−XMP* intermediates using rate constants in Scheme 4 and an enzyme concentration of 4.5 μM, an IMP concentration of 50 μM, and an NAD^+ concentration of 0.8 mM (same conditions that were used for the rapid quench experiment). Approximately 50% of the intermediates accumulating at the steady state are in the form of E−XMP*, which agrees with the rapid quench data (Figure 8A). If this 50% is dissected further, 30% is E−XMP*, 15% is E−XMP*·NADH, and only 5% is trapped in the dead-end E−XMP*·NAD^+ complex.

Implications for MPA Specificity. MPA is a potent inhibitor of human IMPDH but a poor inhibitor of microbial enzymes (20 nM vs 9 μM for human and *T. foetus* IMPDHs, respectively). MPA inhibits by trapping the E−XMP* complex (*11*, *19*, *24*−*26*). Thus, MPA sensitivity will depend on the extent of accumulation of E−XMP* as well as on the affinity of E−XMP* for MPA. A minimal kinetic mechanism of the human type II IMPDH suggests that NADH release is fast and hydrolysis of E−XMP* is rate-limiting at 0.4 s^{-1} (*17*). Therefore, in contrast to *T. foetus* IMPDH (Scheme 4), E−XMP* is the major enzyme form for human IMPDH. This difference in the accumulation of E−XMP* can account for a 3-fold decrease in MPA

sensitivity in *T. foetus* IMPDH.

This result suggests that only a small fraction of the MPA resistance (3-fold out of 450-fold) of *T. foetus* IMPDH is derived from the kinetic properties of the enzyme. Therefore, the structure of the MPA binding sites must be important in determining the selectivity of MPA. Of course, it would not be correct to consider these two mechanisms mutually exclusive. Differences in the structure of the MPA binding site can change the kinetic properties of IMPDH as well as the affinity of MPA. The affinity of E−XMP* for MPA has not been directly measured. However, the E−IMP complex can serve as a model for E−XMP*. Isothermal titration calorimetry experiments perfomed with Chinese hamster IMPDH (98% identical to human IMPDH) indicate that MPA binds to the IMPDH−IMP complex with a K_d of 6 μM (*32*). Fluorescence quenching experiments with *T. foetus* IMPDH indicate that MPA binds to the enzyme−IMP complex with a K_d of 110 μM. These observations indicate that the affinity of MPA for the human enzyme−IMP complex is 18-fold higher than that of the *T. foetus* enzyme−IMP complex. The MPA binding site of *T. foetus* IMPDH contains two residues which differ from human IMPDH. The substitution of these residues with their human counterparts results in a 20-fold increase in MPA sensitivity (J. Digits, unpublished results), which is consistent with the 18-fold increase cited above. These results suggest that the structure of the MPA binding site can account for a significant fraction, but not all, of the MPA sensitivity. The remaining 23-fold difference in MPA sensitivity cannot be accounted for at this time, but must be derived from distal structural elements.

ACKNOWLEDGMENT

We thank Xiaolin Liu and Dr. Wen Wang for computer assistance and helpful discussions. We also acknowledge Dr. Ronald Viola for advice on the Cys319Ser mutant.

REFERENCES

1. Weber, G. (1983) *Cancer Res. 43*, 3466−3492.
2. Streeter, D. G., Witkowski, J. T., Khare, G. P., Sidwell, R. W., Bauer, R. J., Robins, R. K., and Simon, L. N. (1973) *Proc. Natl. Acad. Sci. U.S.A. 70*, 1174−1178.
3. Jackson, R., Weber, G., and Morris, H. P. (1975) *Nature 256*, 331−333.
4. Allison, A. C. (1993) *Immunol. Rev. 136*, 5−28.
5. Cooney, D., Jayaram, H., Gebeyehu, G., Betts, C., Kelley, J., Marquez, V., and Johns, D. (1982) *Biochem. Pharmacol. 31*, 2133−2136.
6. Smith, C., Fontenelle, L., Muzik, H., Paterson, A., Unger, H., Brox, L., and Henderson, J. (1974) *Biochem. Pharmacol. 23*, 2727−2735.
7. Franklin, T., and Cook, J. (1969) *Biochem. J. 113*, 515−524.
8. Hupe, D., Azzolina, B., and Behrens, N. (1986) *J. Biol. Chem. 261*, 8363−8369.
9. Verham, R., Meek, T. D., Hedstrom, L., and Wang, C. C. (1987) *Mol. Biochem. Parasitol. 24*, 1−12.
10. Huete-Perez, J. A., Wu, J. C., Whitby, F. G., and Wang, C. C. (1995) *Biochemistry 34*, 13889−13894.
11. Link, J. O., and Straub, K. (1996) *J. Am. Chem. Soc. 118*, 2091−2092.
12. Anderson, J., and Sartorelli, A. (1968) *J. Biol. Chem. 243*, 4762−4768.
13. Holmes, E., Pehlke, D., and Kelley, W. (1974) *Biochim. Biophys. Acta 364*, 209−217.
14. Carr, S., Papp, E., Wu, J., and Natsumeda, Y. (1993) *J. Biol. Chem. 268*, 27286−27290.
15. Xiang, B., Taylor, J. C., and Markham, G. D. (1996) *J. Biol. Chem. 271*, 1435−1440.
16. Nimmesgern, E., Fox, T., Fleming, M. A., and Thomson, J. A. (1996) *J. Biol. Chem. 271*, 19421−19427.
17. Wang, W., and Hedstrom, L. (1997) *Biochemistry 36*, 8479−8483.
18. Xiang, B., and Markham, G. D. (1997) *Arch. Biochem. Biophys. 348*, 378−382.
19. Sintchak, M. D., Fleming, M. A., Futer, O., Raybuck, S. A., Chambers, S. P., Caron, P. R., Murcko, M. A., and Wilson, K. P. (1996) *Cell 85*, 921−930.
20. Whitby, F. G., Luecke, H., Kuhn, P., Somoza, J. R., Huete-Perez, J. A., Phillips, J. D., Hill, C. P., Fletterick, R. J., and Wang, C. C. (1997) *Biochemistry 36*, 10666−10674.
21. Wang, W., Papov, V. V., Minakawa, N., Matsuda, A., Biemann, K., and Hedstrom, L. (1996) *Biochemistry 35*, 95−101.
22. Beck, J. T., Zhao, S., and Wang, C. C. (1994) *Exp. Parasitol. 78*, 101−112.
23. Farazi, T., Leichman, J., Harris, T., Cahoon, M., and Hedstrom, L. (1997) *J. Biol. Chem. 272*, 961−965.
24. Wu, J. C., Carr, S. F., Antonino, L. C., Papp, E., and Pease, J. H. B. (1995) *FASEB Abstr. 9*, 472.
25. Hedstrom, L., and Wang, C. C. (1990) *Biochemistry 29*, 849−554.
26. Fleming, M. A., Chambers, S. P., Connelly, P. R., Nimmersgen, E., Fox, T., Bruzzese, F. J., Hoe, F. J., Fulghem, J. R., Livingston, D. J., Stuver, C. M., Sintchak, M. D., Wilson, K. P., and Thomson, J. A. (1996) *Biochemistry 35*, 6990−6997.
27. Nijkamp, H. J. J., and De Haan, P. G. (1967) *Biochim. Biophys. Acta 145*, 31−40.
28. Barshop, B. A., Wrenn, R. F., and Frieden, C. (1983) *Anal. Biochem. 130*, 134−145.
29. Lakowicz, J. R. (1983) *Principles of Fluorescence Spectroscopy*, Plenum Press, New York.
30. Cleland, W. W. (1970) in *The Enyzmes* (Boyer, P. D., Ed.) Vol. II, pp 1−66, Academic Press, Inc., New York.
31. Cook, P. (1991) *Enzyme Mechanism from Isotope Effects*, CRC Press, Boca Raton, FL.
32. Bruzzese, F., and Connelly, P. R. (1997) *Biochemistry 36*, 10428−10438.
33. Johnson, K. A. (1992) in *The Enzymes* (Sigman, D. S., Ed.) 3rd ed., Vol. 20, pp 1−61, Academic Press, New York.
34. Halford, S. E. (1972) *Biochem. J. 126*, 727−738.
35. Joseph, D., Petsko, G. A., and Karplus, M. (1990) *Science 249*, 1425−1428.
36. Jencks, W. P. (1987) in *Catalysis in Chemistry and Enzymology* (Jencks, W. P., Ed.) pp 43−111, Dover Publications, Inc., New York.
37. Bruice, T. C., and Lapinski, R. (1958) *J. Am. Chem. Soc. 80*, 2265−2267.
38. Ogilvie, J. W., Tildon, J. T., and Strauch, B. S. (1964) *Biochemistry 3*, 754−758.
39. Dev, I. K., Yates, B. B., Leong, J., and Dallas, W. S. (1988) *Proc. Natl. Acad. Sci. U.S.A. 85*, 1472−1476.
40. LaPat-Polasko, L., Maley, G. F., and Maley, F. (1990) *Biochemistry 29*, 9561−9572.
41. Pazirandeh, M., Chirala, S. S., and Wakil, S. J. (1991) *J. Biol. Chem. 261*, 20946−20952.
42. Guan, K., and Dixon, J. E. (1991) *J. Biol. Chem. 266*, 17026−17030.
43. Whitaker, J. R., Yates, D. W., Bennett, G., Holbrook, J. J., and Gutfreud, H. (1974) *Biochem. J. 139*, 677−697.
44. Hermes, J. D., Morrical, S. W., O'Leary, M. H., and Cleland, W. W. (1984) *Biochemistry 23*, 5479−5488.

BI982305K